Korean Chem. Eng. Res., 61(4), 635-644 (2023)
https://doi.org/10.9713/kcer.2023.61.4.635
PISSN 0304-128X, EISSN 2233-9558

Photocatalytic Degradation and Adsorptive Removal of Tetracycline on Amine-Functionalized Graphene Oxide/ZnO Nanocomposites

Thanh Truong Dang*, Hoai-Thanh Vuong, Sung Gu Kang* and Jin Suk Chung*,†**

**Chemical Engineering, University of Ulsan 93 Daehak-ro, Nam-gu, Ulsan, 44610, Korea*
***Chemistry and Biochemistry, University of California Santa Barbara*
(Received 30 August 2023; Received in revised from 4 October 2023; Accepted 5 October 2023)

Abstract – Due to the rapid development of the livestock industry, particularly due to residual pharmaceutical antibiotics, environmental populations have been negatively affected. Herein, we report a ZnO/melamine-functionalized carboxylic-rich graphene oxide (ZFG) photocatalyst for visible light-driven photocatalytic degradation of tetracycline hydrochloride in aqueous solutions. The properties of the photocatalysts were evaluated by XRD, FTIR, XPS, Fe-SEM, HR-TEM, TGA, Raman spectroscopy, UV-Vis spectroscopy, zeta potential, and electrochemical measurements. The photocatalytic activity was measured using high-performance liquid chromatography. The photocatalytic properties of the ZFG photocatalyst evaluated against the tetracycline hydrochloride (TCH) antibiotic under visible light irradiation showed superior photodegradation of 96.27% within 60 min at an initial pH of 11. The enhancement of photocatalytic degradation was due to the introduction of functionalized graphene, which increases the light-harvesting capability and molecular adsorption capability in addition to minimizing the recombination rate of photogenerated charge carriers due to its role as an electron acceptor and mediator.

Key words: ZnO, Amine functionalized graphene, Photodegradation, Tetracycline, HPLC

1. Introduction

Since the mid-20th century, the rapid growth of society has led to several problems, such as energy shortages and environmental degradation [1]. One such issue is the scarcity of clean water, which plays a pivotal role in human health as well as economic development, due to water pollution associated with extensive, rapid industrialization [2]. Many aquatic pollutants have been identified, but organic dyes, heavy metals, and pharmaceutical compounds have gained considerable attention globally. In this regard, the residue of pharmaceutical antibiotics is a growing concern worldwide [3]. Antibiotics are defined as effective drugs to treat human diseases prompted by bacteria [4]. As a result of intensive antibiotic usage, these compounds may leak into the environment, contributing to the development of bacterial resistance [5]. According to the chemical structures of antibiotic constituents, they are frequently categorized as quinoline, aminoglycosides, macrolides, sulfonamides, and tetracycline (TC) [6].

TC has been widely used as an antibiotic for both humans and livestock for over 50 years because of its activity, low cost, and availability. Based on the structure, tetracycline possesses a high molecular weight of 444 g mol^{-1} as well as carbonyl, amino, and hydroxyl functional groups [7]. With its complex structure, when in water, the ionization equilibrium constants of TC vary, including pK_{a1} at 3.30, pK_{a2} at 7.68, and pK_{a3} at 9.68 [8]. According to previous reports, the presence of TC residue may have detrimental effects due to its acute, chronic toxicity, and the major consequences of antibiotic-resistant bacteria affect human health and the environment [3]. Therefore, removal of TC is a priority throughout the world.

Separation and purification of water due to contaminants have been widely applied for many years. Today, due to their efficiency and green nature, photocatalytic semiconductors are used for degradation of contaminants in water [9]. Many studies have reported the use of semiconductors, such as TiO_2, WO_3, SnO_2, and ZnO, for photocatalytic degradation of organic compounds, where ZnO is emerging as a promising candidate due to its low cost. Nonetheless, recombining electron-hole pairs significantly constrains the efficiency of these materials, limiting practical applications. Thus, higher efficiency photodegradation catalysts are required [10]. To overcome fast electron-hole pair recombination, electron acceptor and mediator materials have been regularly employed to enhance photoactivity. As a two-dimensional material with a high theoretical specific area and unique surface structure, graphene oxide (GO) could serve as an electron acceptor due to its superb electronic conductivity, which facilitates electron transfer and storage [11-13].

In this work, ZnO/Fe_3O_4 nanoparticles cooperate with amine-functionalized graphene oxide as a photocatalyst composite for tetracycline hydrochloride (THC) removal. The results show significantly improved photocatalytic activity when coupling these materials, and nearly complete photodegradation of TCH was obtained in less than 1 h under visible light irradiation at pH 11. This nano-photocatalyst could be a promising material for practical applications.

† To whom correspondence should be addressed.
E-mail: jschung@ulsan.ac.kr

2. Materials and Methods

2-1. Materials

Graphene oxide (GO-V50) was purchased from Standard Graphene (Korea). Oxalic acid (OA), melamine, thionyl chloride ($SOCl_2$), p-benzoquinone (BQ), ammonium oxalate (AO), ethanol (EtOH), isopropyl alcohol (IPA), hydrogen chloride (HCl), and tetracycline hydrochloride (TCH, $C_{22}H_{24}N_2O_8 \cdot HCl$, 95%) were purchased from Daejung Chemicals. Iron(III) chloride hexahydrate ($FeCl_3.6H_2O$), ferrous chloride tetrahydrate ($FeCl_2 \cdot 4H_2O$), zinc chloride ($ZnCl_2$), and ammonium hydroxide solution (NH_4OH, 30-33% NH_3 in H_2O) were purchased from Sigma Aldrich. High-performance liquid chromatography–grade methanol and acetonitrile were purchased from Daejung Chemicals (Korea). All chemicals were used as received without further purification.

2-2. Synthesis of carboxylic-rich graphene oxide (GO-COOH)

First, 1.5 g of GO was dispersed in 1,000 ml of DI water under sonication at high power for 2 h to obtain a homogeneous solution. Subsequently, 10 g of oxalic acid (OA) was added to the above solution with stirring for 24 h. The dispersion was filtered, washed, and redispersed in DI water.

2-3. Synthesis of melamine-functionalized carboxylic-rich graphene oxide (mGO)

The mGO was prepared via amidation reactions between -COOH groups in GO-COOH and -NH_2 groups in melamine using thionyl chloride ($SOCl_2$) as the catalyst. The as-prepared GO-COOH (1.5 mg/mL) was stirred in a three-neck round bottom flask with 20 mL of $SOCl_2$ under reflux conditions overnight to activate -COOH groups before adding aqueous melamine solution (13.5 mg mL^{-1}) and maintaining the reaction conditions for 10 h at 60 ℃. The product, referred to as mGO, was collected and washed to remove unreacted substances, followed by dispersing in 1,000 mL of methanol.

2-4. Synthesis of magnetic ZnO/melamine-functionalized carboxylic-rich graphene oxide

The ZnO/melamine-functionalized carboxylic-rich graphene oxide (mGO/Fe_3O_4/ZnO) was synthesized *in situ* as shown in Scheme 1 and labelled as ZFG. Briefly, 1.215 g of $FeCl_3 \cdot 6H_2O$, 0.46 g of $FeCl_2 \cdot 4H_2O$, 82 mg of $ZnCl_2$, and 1.5 mL of HCl (36.5%) were dissolved in 25 mL of DI water. The prepared solution was poured into the mGO dispersion. Then, NH_4OH solution was dropped into the dispersion to adjust the pH to 10. The dispersion was vigorously stirred under reflux conditions for 2 h before filtering and drying at 80 ℃ in an oven.

2-5. Evaluation of photocatalytic activity

For the photocatalytic activity study, 12.5 mg of the as-synthesized catalysts was dispersed into 20 mL of TCH solution (20 ppm). The mixture was stirred for 30 min in a dark box to achieve adsorption-desorption equilibrium. Then, four led lamps (25 W) were activated to investigate the photocatalytic activity under visible light for 60 min. For each analysis, 1 mL of TCH solution was periodically collected at specific time intervals and filtered through a syringe filter with a pore size of 45 μm for TCH analysis. For confirmation, ZnO and mGO were used instead of ZFG as a comparison experiment. To further study the primary reactive species in the photodegradation of TCH, radical scavenging experiments were conducted using 1 mM

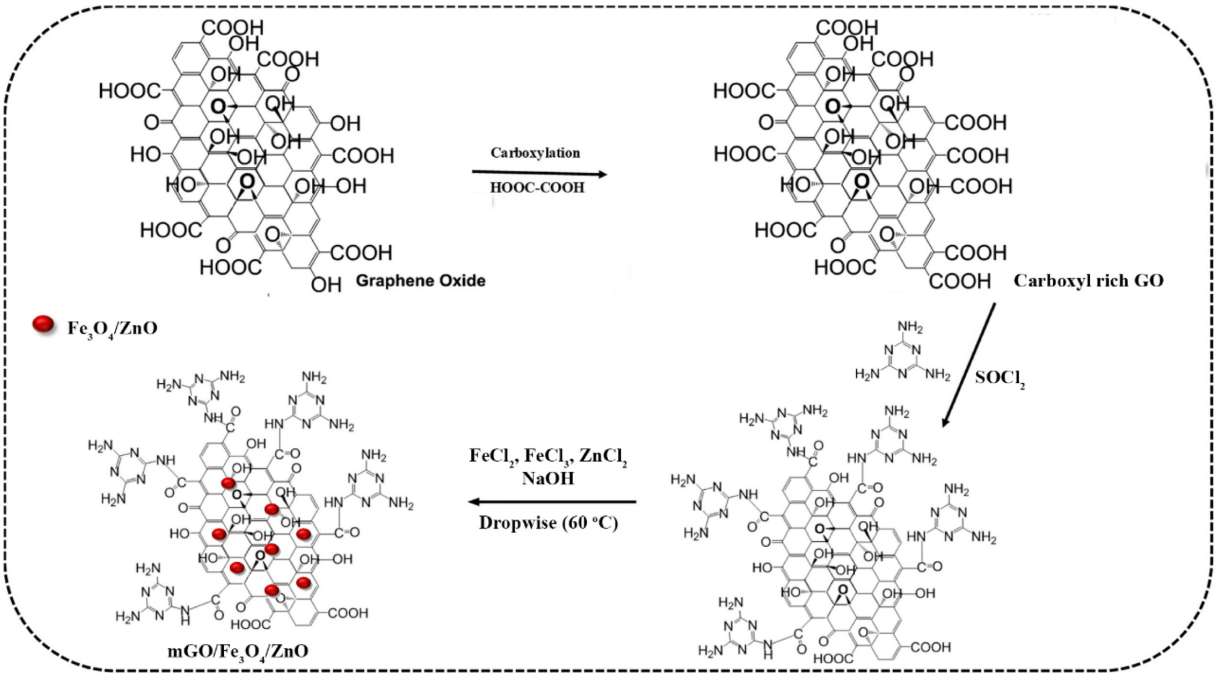

Scheme 1. The general schematic synthesis of ZFG (mGO/Fe_3O_4/ZnO).

of p-benzoquinone (BQ), 3 mM of ammonium oxalate (AO), 1 mL of ethanol (EtOH), and 1 mL of isopropyl alcohol (IPA) as $\cdot O_2^-$, h^+, e^-, and $\cdot OH$ scavengers, respectively. The removal efficiency of TCH was calculated using the following formula:

$$E = 100\frac{C - C_0}{C_0} \quad (1)$$

where E is the removal efficiency, and C_0 and C are the initial concentration of TCH and the concentration at a specified time in the solution, respectively.

2-6. Analytical methods

TCH was analyzed using a high-performance liquid chromatography system (Agilent 1200) equipped with a variable wavelength detector (VWD) and an Eclipse Plus C18 analytical column (4.6 × 250 mm, 5 μm). Oxalic acid (0.01 M), acetonitrile, and methanol were employed as a mobile phase for TCH analysis in an isocratic program at a ratio of 70:28:2. The flow rate and column temperature were kept at 0.8 mL min^{-1} and 25 ℃, while the injection volume and wavelength were set at 20 μL and 355 nm, respectively. The chromatograms of TCH show a retention time of about 4.2 min before and after irradiation.

3. Results and Discussion

3-1. Catalyst characterization

The morphologies and compositions of ZnO and ZFG were captured by FE-SEM and HR-TEM with energy-dispersive spectrometry (EDS) analysis. As shown in Fig. 1a, ZnO had a typical particle structure, while ZFG possessed a layer structure of 2D graphene material covered by uniformly distributed ZnO and Fe_3O_4 nanoparticles. At higher resolution, the nanoparticles (ZnO and Fe_3O_4) appeared as a moss-like shape on the surface of the graphene layer (Fig. 1c). Fig. 1d shows a high-resolution image of the nanoparticles with a crystalline lattice, in which the d-spacing was determined via high-resolution inverse FFT images (Fig. 1k, l, m, and n).

The crystal structures and phase purity values of the pristine ZnO and ZFG samples were analyzed by XRD (Fig. 2). Fig. 2b shows the XRD patterns of ZFG in which three sets of XRD patterns were observed in respective association with functionalized graphene, ZnO, and Fe_3O_4. The peak of functionalized graphene is displayed at 22.83° [14]. The typical hexagonal wurtzite structure with $P6_3mc$ symmetry of ZnO nanoparticles showed peaks at 2θ values of 31.66°, 34.28°, 36.16°, 47.46°, 56.35°, 62.82°, 66.45°, 67.84°, and

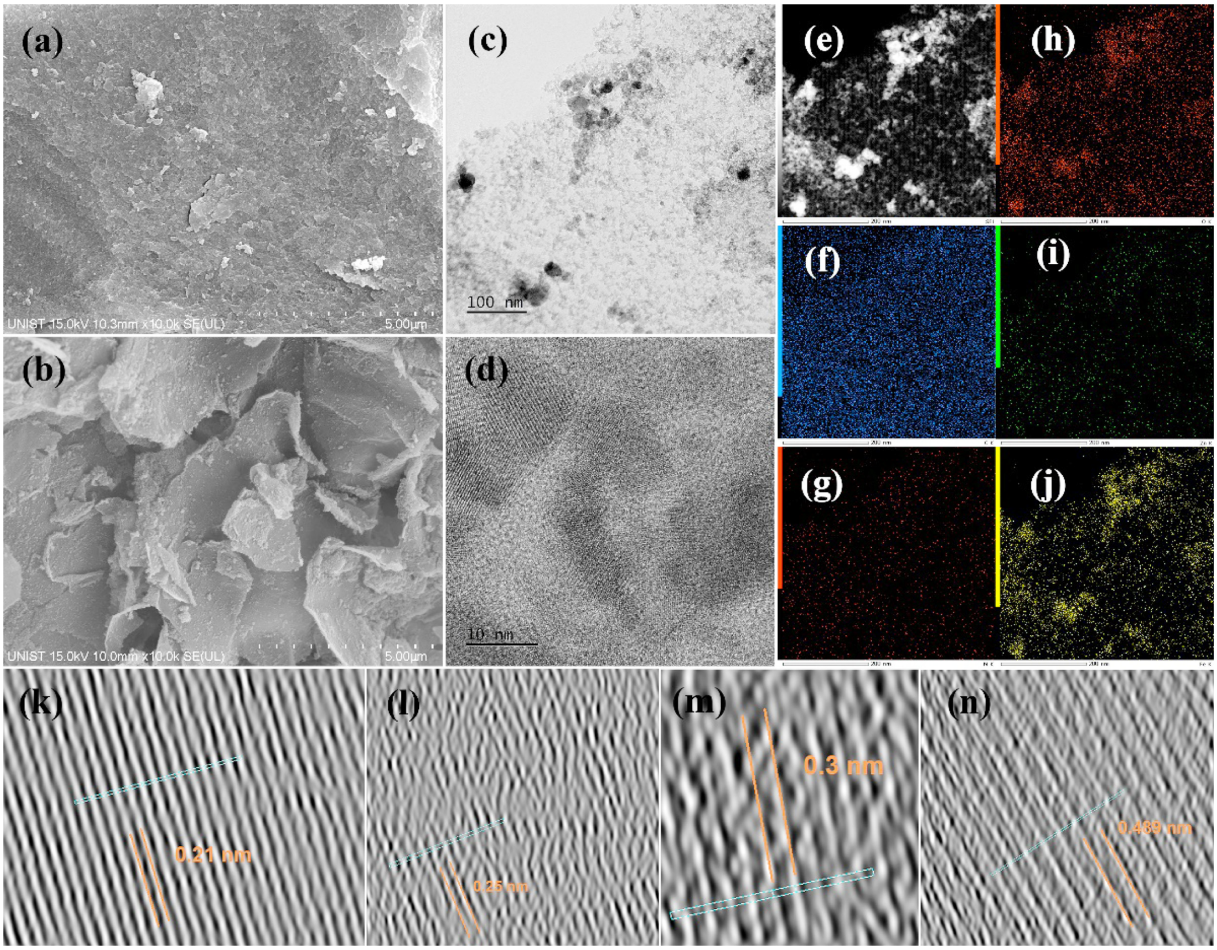

Fig. 1. FE-SEM images of (a) ZnO and (b) ZFG. (c, d) HR-TEM images of ZFG at different resolutions. (e) HR-TEM image of ZFG, corresponding to the EDS images of (f) C, (g) N, (h) O, (i) Zn, and (j) Fe. High-resolution inverse FFT images (IFFT) from (d), showing d-spacings of Zn nanoparticles of (k) 0.21 nm, (l) 0.25 nm, and (m) 0.3 nm and (n) an Fe (111) d-spacing of 0.489 nm.

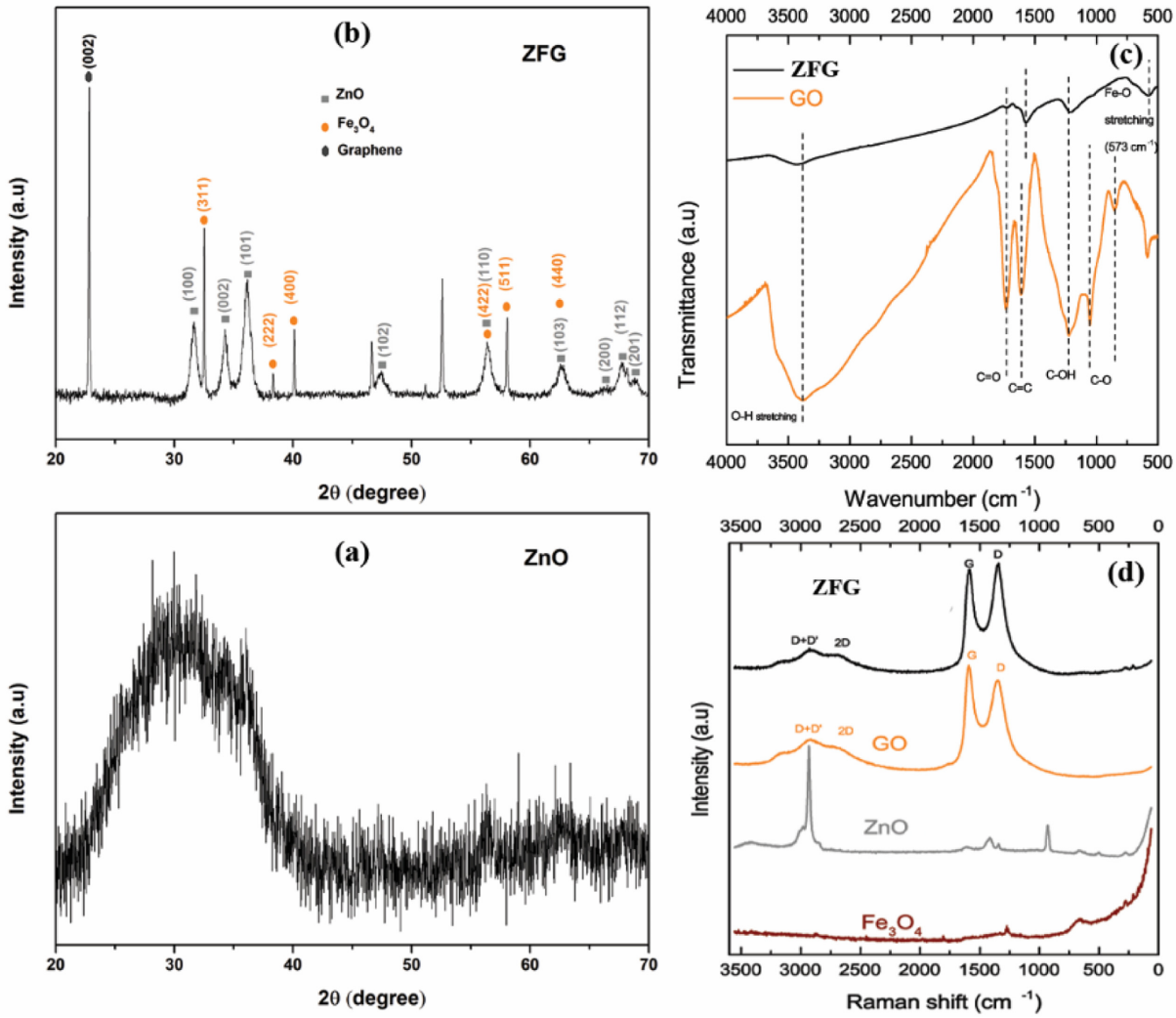

Fig. 2. XRD spectra, FTIR spectra, and Raman spectra of resultant samples.

68.87°, which represent (100), (002), (101), (102), (110), (103), (200), (112), and (201) planes, respectively. These peaks are well matched with the JCPDS, File No. 036-1451 [15], while the Fe_3O_4 diffraction peaks are matched with characteristic diffractions of the Fe_3O_4 inverse spinel structure (PDF No. 89-0691) [16]. In contrast, pristine ZnO did not show any sharp peaks due to the low crystallinity of its quantum dots (Fig. 2a). The functional groups and graphitic structure of the as-prepared samples were analyzed by FTIR spectroscopy and Raman spectroscopy, respectively (Fig. 2c, Fig. 2d).

XPS was used to investigate the electronic structure and surface composition of the ZnO and ZFG samples. The deconvoluted XPS spectrum of C 1s in ZFG (Fig. 3f) shows three fitted peaks at binding energies of 284.5, 285.8, and 288.2 eV, which can be related to C–C, C–O, and C=O chemical bonds, respectively. The core level of the Fe 2p XPS spectrum shows fitted peaks at 711.03 eV (Fe $2p_{3/2}$) and 725.01 eV (Fe $2p_{1/2}$), confirming successful generation of Fe_3O_4 (Fig. 3e). As shown in Fig. 3a and Fig. 3b, there is one peak centered at ca. 1,022 eV, corresponding to Zn $2p_{3/2}$, indicating a normal state of Zn^{2+} in ZnO nanoparticles. Another peak is centered at ca. 1,044.5 eV, corresponding to the binding energy of Zn $2p_{1/2}$. In addition, the O 1s core-level spectrum shows two deconvoluted peaks at ca. 532.39 eV and 531.11 eV, which are related to adsorbed oxygen and hydroxide, respectively, and attributed to the lattice oxygen in the samples.

The optical properties of the as-prepared samples were studied by UV-Vis analysis. As observed in Fig. 4a, ZnO and ZFG samples have similar optical characteristics. However, ZFG shows a much higher light absorption ability, which means that ZFG exhibits better light harvesting capability. Thermogravimetric analysis (TGA) revealed the high thermal stability of ZFG compared to ZnO (Fig. 4b). Zeta potential measurements showed a shift of charge from positive in ZnO to negative in ZFG due to the introduction of graphene, which is beneficial for adsorption and photodegradation. This finding is consistent with adsorption in the dark of the resulting samples (Fig. 4e and Fig. 4f). EIS measurements were carried out to investigate the charge transfer resistance at the catalyst electrode/electrolyte interface. A smaller radius of the EIS Nyquist plot reflects a smaller resistance for charge carrier transfer at the catalyst/electrolyte interface. Compared

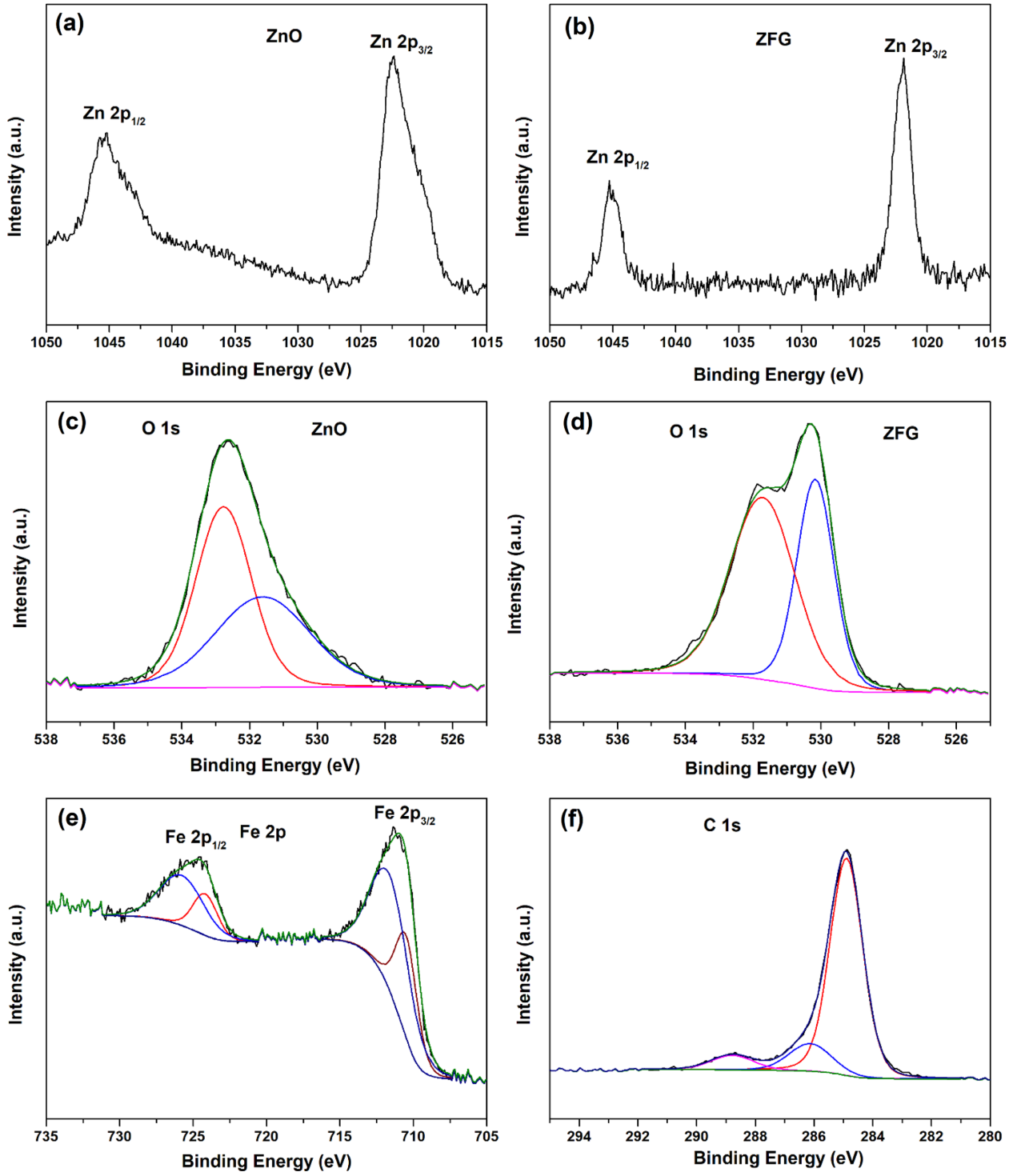

Fig. 3. XPS spectra of ZnO: (a) Zn 2p and (c) O 1s; ZFG: (b) Zn 2p, (d) O 1s, (e) Fe 2p, and (f) C 1s.

to ZnO, the ZFG sample shows a much smaller radius in the EIS Nyquist plot, demonstrating lower charge transfer resistance from the catalyst surface to reactant molecules (Fig. 4d).

3-2. Photocatalytic performance

3-2-1. Effect of catalyst dosage

The effect of the dosage of photocatalyst was investigated in this study with five amounts of 5, 7.5, 10, 12.5, and 15 mg. It has been suggested that the quantity of nano-photocatalyst could be essential for the reaction under light irradiation because of the direct relationship to absorption of molecules on the catalyst surface [17]. As in Figs. 5a and Fig. 5b, with increasing catalyst dosage, an increase of removal efficiency of tetracycline was recorded. The most efficient catalyst amount was 12.5 mg, with a removal efficiency of 91.61% after lighting for 1 h. As the distribution of TCH on the adsorption sites of the photocatalyst was not saturated with a small amount of catalyst,

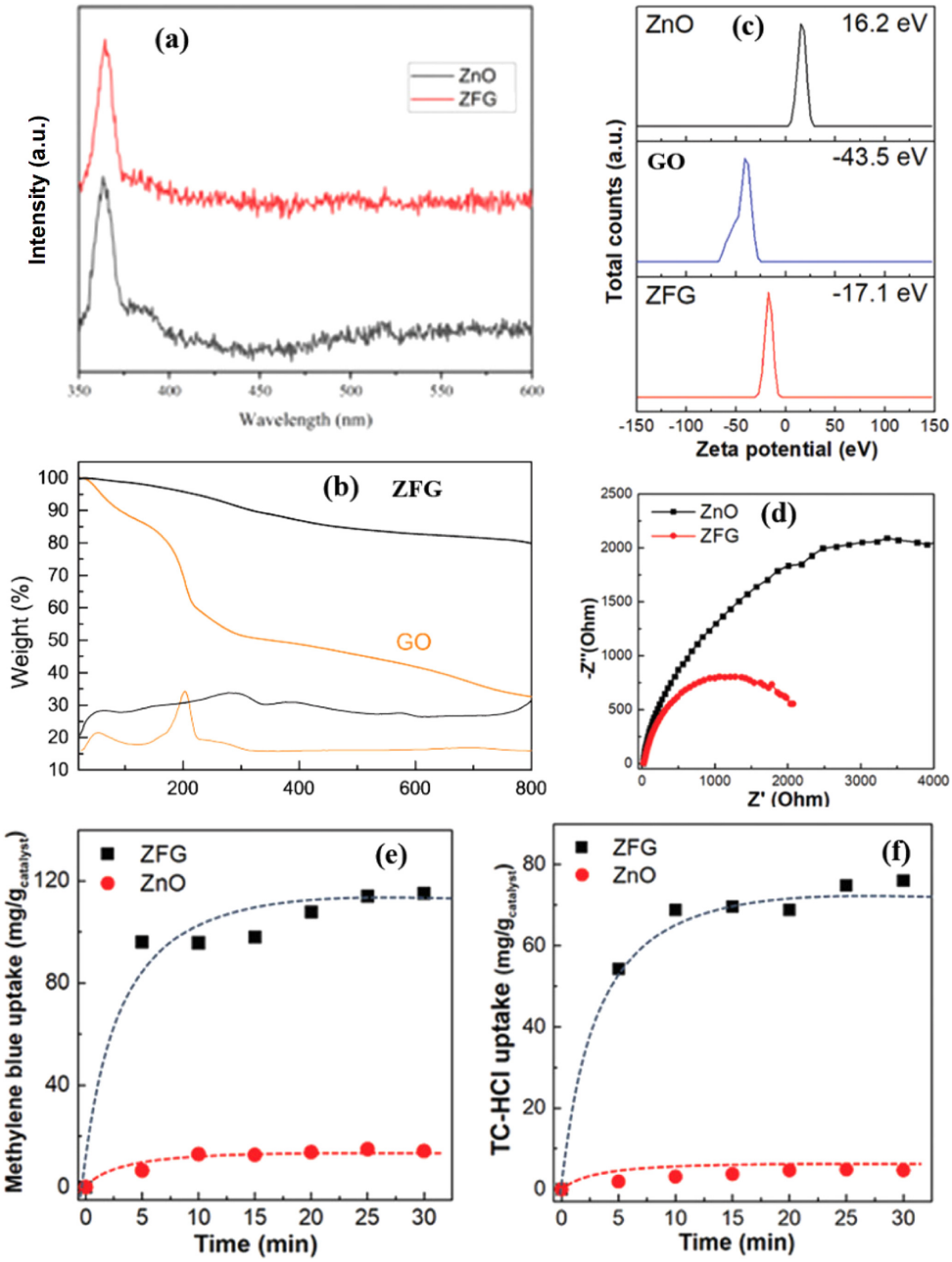

Fig. 4. (a) UV-Vis spectra, (b) TGA spectra, (c) Zeta potential, (d) EIS Nyquist plots, (e) and (f) UV-Vis absorbance of the resulting samples in the dark.

increasing the catalyst amount could lead to greater absorption capability and result in higher removal efficiency [18]. As the catalyst quantity reached 15 mg, the removal efficiency decreased slightly to 90.45% since the solution gradually became opaque, leading to difficulty in light penetration [19].

Fig. 5c and Fig. 5d present the photocatalytic kinetics of TCH under visible light irradiation based on the pseudo-first-order kinetic model:

$$\ln\left(\frac{C}{C_0}\right) = -kt \quad (2)$$

where C is the concentration of TCH in the solution at a specified time t, C_0 is the initial concentration of TCH after the absorption-desorption equilibrium, and k is the apparent rate constant (min^{-1}).

Based on formula (2), the empirical rate constants of the solution containing 20 ppm of TCH are 0.0189, 0.0181, 0.0183, 0.0176, and 0.0138 min^{-1} with catalyst amounts of 5, 7.5, 10, 12.5, and 15 mg, respectively. These results show that the shielding effect plays a critical role in the decrease of these constants. As mentioned, increased catalyst loading restricts light penetration into the solution, increasing the absorption capability but decreasing the photocatalytic activity due to the difficult light transmittance. Moreover, overloading of photocatalysts could hamper the degradation efficiency because of reduced interactions between TCH and hydroxyl radicals [17].

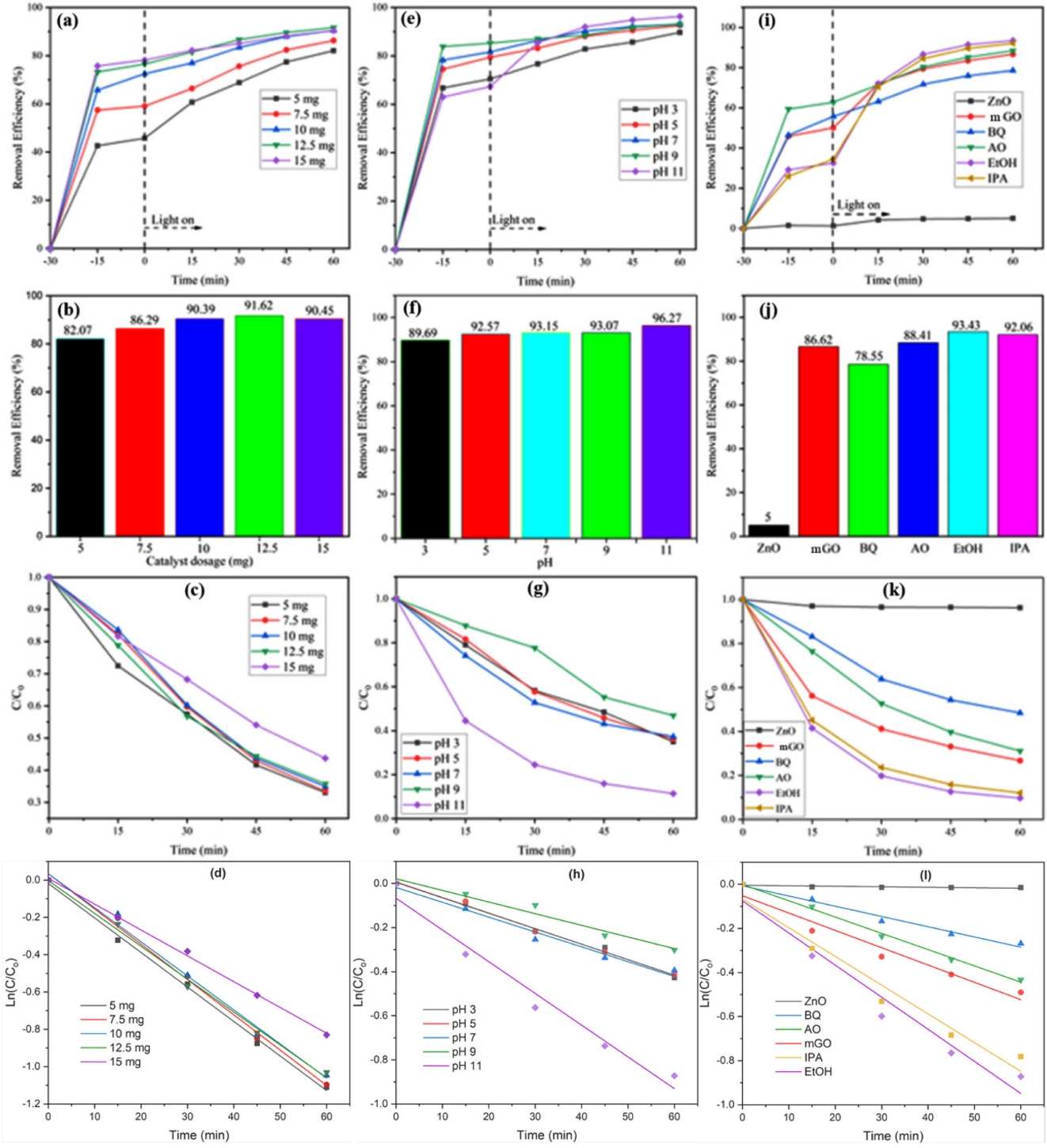

Fig. 5. (a) Dark absorption and photocatalytic degradation of prepared samples with various catalyst dosages and the (b) removal efficiency corresponding to the (c, d) photodegradation kinetics plots of various catalyst dosages. (e) pH dependence and (f) removal efficiency corresponding to the (g, h) photodegradation kinetics plots. (i) Dark absorption and photocatalytic degradation of prepared samples in the presence of various scavengers. (j) Removal efficiency corresponding to the (k, l) photodegradation kinetics plots.

Consequently, to obtain the best TCH removal in aqueous solution, 12.5 mg of catalyst was selected for the subsequent experiments to combine adsorptive and photocatalytic activities.

3-2-2. Effect of initial pH

The initial pH is an imperative parameter for adsorption and photodegradation of organic pollutants since it exerts an impact not only on the photocatalyst surface electrical charge, but also the ionization state of the catalyst surface [5]. From Fig. 5e, the absorption capability of TCH at pH 9 was greater than that of the counterparts. In contrast, at pH 11, the empirical data show that TCH was absorbed at the lowest rate. Meanwhile, in the irradiating process, the trend changed

Table 1. The photodegradation of tetracycline contaminant performance of ZnO/graphene-based composites

Contaminant	Photocatalyst	Light source	Photodegradation performance (%)	Ref.
TC	MZ	Simulated light (1 kW m^{-2})	74	[27]
	SDS/ZnO	350 W xenon lamp ($\lambda > 420$ nm)	49.0	[28]
	ZnO/rGO-2	6 W LED lamp (UV light)	95.4	[29]
	RGO-ZnO	UV light	82	[30]
	ZFG	4 × 25 W LED (Commercial)	96.2	This work

to significant degradation of TCH at pH 11. From Fig. 5e, Fig. 5f, Fig. 5g, and Fig. 5h, the removal efficiency of TCH at various pH values gradually increased from 89.69 to 96.27%, where the apparent rate constants ranged from 0.0173 to 0.0358 min^{-1}. At pH 11, the degradative reaction occurred rapidly, allowing greater efficiency with respect to photodegradation. From previous studies, it has been asserted that, while TC is predominant at pH < 4, it would be present in one of four forms depending on the initial pH of the dissolving solution; these forms are the protonated form (TC^+) at pH 4-7.5, amphoteric ion ($TC^{\pm}$) and negative ion form (TC^-) at pH 7.5-10, and dianion form (TC^{2-}) at higher pH due to its amphoteric molecules [8, 20]. Under lower pH values, in the presence of HCl, acidification produces ClO^- radicals. These radicals are less reactive than hydroxyl radicals, which have been considered a main factor in the aquatic photodegradation of organic contaminants through the reaction of Cl^- and $\cdot OH$. In addition, there is high competition between TC and Cl^- to react with $\cdot OH$, resulting in lower photocatalytic performance at lower pH [21,22]. This is contradictory with acidic conditions, as it is believed that the growth of OH^- ions under alkaline conditions induces more $\cdot OH$ radicals, rendering a huge contribution to the photodegradation of tetracycline [23]. Therefore, the optimal pH in this study was 11, which is well matched with related research [24]. As compared, the photodegradation of tetracycline contaminants performance of ZnO/graphene-based composites in the literature is listed in Table 1.

3-2-3. Comparison samples investigations and possible photocatalytic mechanism

For further confirmation, ZnO and mGO were employed under the same experimental conditions to validate the efficiency of the catalysts. The results in Fig. 5i, Fig. 5j, Fig. 5k, and Fig. 5l illustrate lower photocatalytic activity under light radiation with ZnO, where the apparent rate constant is 0.0006 min^{-1}, which is significantly lower than that of mGO. The phenomenon indicates the effectiveness of combining two materials to enhance the photocatalytic properties of ZnO.

In terms of the roles of free radicals in photocatalysis that could be used to analyze the electron migration mechanism, capture experiments were conducted with four agents, benzoquinone (BQ), ammonium oxalate (AO), ethanol (EtOH), and isopropyl alcohol (IPA). The figures show superoxide radicals ($\cdot O_2^-$) as a crucial factor in the photoreaction stage, with the removal efficiency decreasing to 78.55%, and that addition of AO quenches h^+ radicals, prohibiting photodegradation. In addition, slight reductions were recorded when pouring EtOH and IPA into the system. Consequently, the order of the role of free radicals could be $\cdot O_2^- > h^+ > \cdot OH > e^-$.

It is widely accepted that, under irradiation, the electrons from the valance band (VB) of ZnO nanoparticles are excited and move into the conduction band (CB), allowing the formation of a large number of holes at the VB. Furthermore, a reaction between photogenerated electrons and the oxygen-functioning groups on the GO surface can occur in which GO is reduced into rGO. Because the Fermi level of the CB of ZnO (-4.05 eV) is higher than that of reduced graphene oxide (-4.42 eV), a strong interaction between ZnO and reduced graphene oxide causes a change of the generated electrons from the CB of ZnO to the CB of reduced graphene oxide. In this case, reduced graphene oxide acts as an electron acceptor to facilitate the migration of electrons into ZnO nearby to form superoxide radicals ($\cdot O_2^-$) by reducing the molecular adsorbed oxygen, which could further react with hydronium ions to generate hydroxyl radicals [12, 17,25]. Some researchers postulated that the valance holes (h^+) could further react with water molecules to form hydroxyl radicals, which bind to the surface of the catalysts [26]. The chain reactions are as follows:

$$ZnO + h\nu \rightarrow ZnO\left(e_{CB}^- + h_{VB}^+\right) \quad (3)$$

$$e_{CB}^- + GO \rightarrow rGO\left(e_{CB}^-\right) \quad (4)$$

$$rGO\left(e_{CB}^-\right) + ZnO_{nearby} \rightarrow ZnO_{nearby}\left(e_{CB}^-\right) + rGO \quad (5)$$

$$ZnO_{nearby}\left(e_{CB}^-\right) + O_2 \longrightarrow \cdot O_2^- + ZnO_{nearby} \quad (6)$$

$$ZnO\left(h_{VB}^+\right) + H_2O \longrightarrow \cdot OH + H^+ + ZnO \quad (7)$$

$$ZnO\left(h_{VB}^+\right) + OH^- \rightarrow ZnO + \cdot OH \quad (8)$$

$$\cdot O_2^- + H^+ \rightarrow \cdot OOH \rightarrow \cdot OH \quad (9)$$

$$\cdot O_2^- + \cdot OH + TCH \rightarrow CO_2 + H_2O + others \quad (10)$$

4. Conclusion

ZnO nanoparticles supported on melamine-functionalized carboxylic-rich graphene oxide photocatalyst for antibiotic TCH degradation under irradiation using a commercial led light were systematically studied. The introduction of mGO not only increased the light-harvesting capability, but also acted as a substrate for surface distribution of ZnO nanoparticles, which supports enhanced photocatalytic performance. The photocatalytic activity toward TCH degradation

was optimized by screening the effects of catalyst dosage and initial pH and by conducting comparison sample investigations. The ZFG photocatalyst resulted in photocatalytic degradation of tetracycline hydrochloride antibiotic under commercial LED light irradiation with a superior photodegradation greater than96% within 60 min at an initial pH of 11. The facile large-scale synthesis process and low cost of ZnO photocatalysts suggest ZFG as a potential candidate for visible light-driven photocatalytic degradation of antibiotics.

Acknowledgment

This study was supported by the Regional Innovation Strategy (RIS) through the Ministry of Education (MOE) (2021RIS-003).

References

1. Zhou, C., Lai, C., Xu, P., Zeng, G., Huang, D., Li, Z., Zhang, C., Cheng, M., Hu, L., Wan, J., Chen, F., Xiong, W. and Deng, R., "Rational Design of Carbon-Doped Carbon Nitride/$Bi_{12}O_{17}Cl_2$ Composites: A Promising Candidate Photocatalyst for Boosting Visible-Light-Driven Photocatalytic Degradation of Tetracycline," *ACS Sustainable Chemistry & Engineering*, **6**, 6941-6949 (2018).
2. Chen, X., Xu, X., Cui, J., Chen, C., Zhu, X., Sun, D. and Sun, D., "Visible-light Driven Degradation of Tetracycline Hydrochloride and 2,4-dichlorophenol Byfilm-like N-carbon@N-ZnO Catalyst with Three-dimensional Interconnected Nanofibrous Structure," *J. Hazardous Materials*, **392**, 122331(2020).
3. Tung, M. H. T., Cam, N. T. D., Thuan, D. V., Quan, P. V., Hoang, C. V., Phuong, T. T. T., Lam, N. T., Tam, T. T., Chi, N. T. P. L., Lan, N. T., Thoai, D. N. and Pham, T.-D., "Novel Direct Z-scheme AgI/N–TiO_2 Photocatalyst for Removal of Polluted Tetracycline Under Visible Irradiation," *Ceramics International*, **46**, 6012-6021(2020).
4. Chen, G., Yu, Y., Liang, L., Duan, X., Li, R., Lu, X., Yan, B., Li, N. and Wang, S., "Remediation of Antibiotic Wastewater by Coupled Photocatalytic and Persulfate Oxidation System: A Critical Review," *J. Hazardous Materials*, **408**,124461(2020).
5. Saadati, F., Keramati, N. and Ghazi, M. M., "Influence of Parameters on the Photocatalytic Degradation of Tetracycline in Wastewater: A Review," *Critical Reviews in Environmental Science and Technology*, **46**, 757-782(2016).
6. Das, P., Pan, A., Chakraborty, K., Pal, T. and Ghosh, S., "RGO-ZnSe Photocatalyst towards Solar-Light-Assisted Degradation of Tetracycline Antibiotic Water Pollutant," *ChemistrySelect*, **3**, 10214-10219(2018).
7. Thi, V. H. T. and Lee, B.-K., "Great Improvement on Tetracycline Removal Using ZnO Rod-activated Carbon Fiber Composite Prepared with a Facile Microwave Method," *J. Hazardous Materials*, **324**, 329-339(2017).
8. Zhao, C., Hong, P., Li, Y., Song, X., Wang, Y. and Yang, Y., "Mechanism of Adsorption of Tetracycline–Cu Multi-pollutants by Graphene Oxide Mechanism of Adsorption of Tetracycline–Cu Multi-pollutants by Graphene Oxide," *J. Chemical Technology and Biotechnology,* **94**, 1176-1186(2019).
9. Du, Q., Wu, P., Sun, Y., Zhang, J. and He, H., "Selective Photodegradation of Tetracycline by Molecularly Imprinted ZnO@Selective Photodegradation of Tetracycline by Molecularly Imprinted ZnO@," *Chemical Engineering J.,* **390**, 129350(2020).
10. Yan, X., Yan, X., Ning, G., Li, J., Ai, T., Su, X. and Wang, Z., "A Novel Poly(triazine imide) Hollow Tube/ZnO Heterojunction for Tetracycline Hydrochloride Degradation Under Visible Light Irradiation," *Advanced Powder Technology*, **30**, 359-365(2019).
11. Xu, F., Yuan, Y., Wu, D., Zhao, M., Gao, Z. and Jiang, K., "Synthesis of ZnO/Ag/graphene Composite and its Enhanced Photocatalytic Efficiency," *Materials Research Bulletin*, **48**, 2066-2070(2013).
12. Thinh, D. B., Tien, N. T., Dat, N. M., Phong, H. H. T., Giang, N. T. H., Tai, L. T., Oanh, D. T. Y., Nam, H. M., Phong, M. T. and Hieu, N. H., "Improved Photodegradation of p-nitrophenol From Water Media Using Ternary $MgFe_2O_4$-doped TiO_2/reduced Graphene Oxide," *Synthetic Metals*, **270**, 116583(2020).
13. Zhu, P., Chen, Y., Duan, M., Liu, M., Zou, P. and Zhou, M., "Enhanced Visible Photocatalytic Activity of Fe-Cu-ZnO/Graphene Oxide Photocatalysts for the Degradation of Organic Dyes," *Canadian J. Chemical Engineering*, **96**, 1479-1488(2018).
14. Sharma, P., Kumar, N., Chauhan, R., Singh, V., Srivastava, V. C., Sharma, P., Kumar, N., Chauhan, R., Singh, V. and Srivastava, V. C., "Growth of Hierarchical ZnO Nano Flower on Large Functionalized rGO Sheet for Superior Photocatalytic Mineralization of Antibiotic," *Chemical Engineering J.*, **392**, 123746(2020).
15. Anirudhan, T. S. and Deepa, J. R., "Nano-zinc Oxide Incorporated Graphene Oxide/nanocellulose Composite for the Adsorption and Photo Catalytic Degradation of Ciprofloxacin Hydrochloride From Aqueous Solutions," *J. Colloid and Interface Science,* **490**, 343-356(2017).
16. Munawar, T., Mukhtar, F., Nadeem, M. S., Mahmood, K., Hussain, A., Ali, A., Arshad, M. I., un Nabi, M. A. and un Nabi, M. A., "Structural, Optical, Electrical, and Morphological Studies of rGO Anchored Direct Dual-Z-Scheme ZnO-Sm_2O_3–Y_2O_3 Heterostructured Nanocomposite: Direct Dual-Z-scheme ZnO-Sm_2O_3–Y_2O0 Heterostructured Nanocomposite," *Solid State Sciences*, **106**, 106307(2020).
17. Jesús, J. L.-P., Manuel, S.-P., Carla, V. G.-P., José, R.-U., "Photodegradation of Tetracyclines in Aqueous Solution by Using UV and UV/H_2O_2 Oxidation Processes," *J. Chemical Technology and Biotechnology*, **85**, 1325-1333(2010).
18. Alireza, N.-E. and Arezoo, S., "Enhancement of the Photocatalytic Activity of Ferrous Oxide by Doping Onto the Nanoclinoptilolite Particles Towards Photodegradation of Tetracycline," *Chemosphere,* **107**, 136-144(2014).
19. Zyoud, A. H., Zubi, A., Zyoud, S. H., Hilal, M. H., Zyoud, S., Qamhieh, N., Hajamohideen, A. and Hajamohideen, A., "Kaolin-supported ZnO Nanoparticle Catalysts in Self-sensitized Tetracycline Photodegradation: Zero-point Charge and pH Effects," *Applied Clay Science*, **182**, 105294(2019).
20. Demircivi, P. and Demircivi, P., "Visible-light-enhanced Photoactivity of Perovskite-type W-doped $BaTiO_3$ Photocatalyst for Photodegradation of Tetracycline," *J. Alloys and Compounds*, **774**, 795-802(2019).
21. Ashok Kumar, K. V., Lakshminarayana, B, Suryakala, D. and

Subrahmanyam, Ch., "Reduced Graphene Oxide Supported ZnO Quantum Dots for Visible Light-induced Simultaneous Removal of Tetracycline and Hexavalent Chromium," *RSC Advances*, **10**, 20494-20503(2020).
22. Wu, F., Zhou, F., Zhu, Z., Zhan, S. and He, Q., "Enhanced Photocatalytic Activities of Ag_3PO_4/GO in Tetracycline Degradation," *Chemical Physics Letters*, **724**, 90-95(2020).
23. Abdel-Mottaleb, M. M., Khalil, A., Karim, S. A., Osman, T. A., and Khattab, A., "High Performance of PAN/GO-ZnO Composite Nanofibers for Photocatalytic Degradation Under Visible Irradiation," *J. of the Mechanical Behavior of Biomedical Materials*, **96**, 118-124(2020).
24. Kumar, K. V. A., Lakshminarayana, B., Suryakala, D., Subrahmanyam, C., "Reduced Graphene Oxide Supported ZnO Quantum Dots for Visible Light-induced Simultaneous Removal of Tetracycline and Hexavalent Chromium," *RSC Advances*, **10**, 20494-20503(2020).
25. Wu, F., Zhou, F., Zhu, Z., Zhan, S. and He, Q., "Enhanced Photocatalytic Activities of Ag_3PO_4/GO in Tetracycline Degradation," *Chemical Physics Letters*, **724**, 90-95(2020).
26. Abdel-Mottaleb, M. M., Khalil, A., Karim, S., Osman, T. A. and Khattab, A., "High Performance of PAN/GO-ZnO Composite Nanofibers for Photocatalytic Degradation Under Visible Irradiation," *J. of the Mechanical Behavior of Biomedical Materials*, **96**, 118-124(2019).
27. Qiao, D., Li, Z., Duan, J. and He, X., "Adsorption and Photocatalytic Degradation Mechanism of Magnetic Graphene Oxide/ZnO Nanocomposites for Tetracycline Contaminants," *Chemical Engineering J.*, **400**, 125952(2020).
28. Jia, K., Liu, G., Lang, D.-N., Chen, S.-F., Yang, C., Wu, R.-L., Wang, W. and Wang, J.-D., "Degradation of Tetracycline by Visible Light Over ZnO Nanophotocatalyst," *J. of the Taiwan Institute of Chemical Engineers*, **136**, 104422(2022).
29. Gang, R., Xu, L., Xia, Y., Zhang, L., Wang, S., Li, R., "Facile One-step Production of 2D/2D ZnO/rGO Nanocomposites under Microwave Irradiation for Photocatalytic Removal of Tetracycline," *ACS Omega*, **6**, 3831-3839(2021).
30. Kar, S., Chakraborty, K., Pal, T. and Ghosh, S., "Enhanced Photocatalytic Degradation of Tetracycline by RGO-ZnO Composite, *AIP Conference Proceedings*, 2265, 030134(2020).

Authors

Thanh Truong Dang: Doctor, Department of Chemical Engineering, University of Ulsan, Ulsan 44610, Korea; michael.dang@live.com

Hoai-Thanh Vuong: Master, Department of Chemistry and Biochemistry, University of California Santa Barbara (UCSB), Santa Barbara, CA 03106, USA; hoaithanhhc16ktmb@gmail.com

Sung Gu Kang: Professor, Department of Chemical Engineering, University of Ulsan, Ulsan 44610, Korea; sgkang@ulsan.ac.kr

Jin Suk Chung: Professor, Department of Chemical Engineering, University of Ulsan, Ulsan 44610, Korea; jschung@ulsan.ac.kr